CrossMark

ORIGINAL ARTICLE

Biomechanical behavior of human crural fascia in anterior and posterior regions of the lower limb

Piero G. Pavan[1,3] · **Paola Pachera**[1,3] · **Carla Stecco**[2,3] · **Arturo N. Natali**[1,3]

Abstract The present work focuses on the numerical modeling of the mechanical behavior of the crural fascia, the deep fascia enwrapping the lower limb muscles. This fascia has an important biomechanical role, due to its inter-action with muscles during contraction and its association with pathological events, such as compartment syndrome. The mechanical response of the crural fascia is described by assuming a hyperelastic fiber-reinforced constitutive model, with families of fibers disposed according to the spatial disposition of the collagen network, as shown in histological analyses. A two-dimensional finite element model of a lower limb transversal section has been devel-oped to analyze deformational behavior, with particular attention on interaction phenomena between crural fascia and enwrapped muscles. The constitutive model adopted for the crural fascia well fits experimental data taken along the proximal–distal and medial–lateral directions. The finite element analysis allows for interpreting the relation between change in volume and pressure of muscle com-partments and the crural fascia deformation.

Keywords Crural fascia · Constitutive modeling · Hyperelasticity · Finite element analysis · Compartment syndrome

✉ Piero G. Pavan
piero.pavan@unipd.it

1 Department of Industrial Engineering, University of Padova, Via G. Marzolo 9, 35131 Padova, Italia, Italy

2 Department of Molecular Medicine, University of Padova, via A. Gabelli 63 3, 35131 Padova, Italy

3 Centre of Mechanics of Biological Materials, University of Padova, Via G. Colombo 3, 35131 Padova, Italy

1 Introduction

A fascial system spans different regions creating compart-ments that envelope and separate different groups of mus-cles [4, 21]. The composition [3, 19, 21–23] and continu-ity give to the fascial system a fundamental and active role in muscle contraction coordination, in load transposition among adjacent regions and in proprioceptive functions [24, 25].

The attention is here focused on the crural fascia, a structure that extends from the knee to the ankle joint cre-ating three compartments and enveloping the muscles of the lower limb in the anterior, the posterior and the lateral compartment. The crural fascia is composed of two dense connective tissue layers separated by a thin layer of loose connective tissue. Experimental investigations [21] showed that dense layers can have a mean thickness of 277.8 μm (SD = 86.1 μm) and the loose layer a mean thickness of 43 μm (SD = 12 μm). Each layer of dense tissue is rein-forced by a family of collagen fibers oriented along a spe-cific direction and forming an angle of about 80° with the fibers of the adjacent layer [23], determining mechanical anisotropic characteristics. The fibers show a wave arrange-ment responsible for a nonlinear behavior characterized by typical stiffening [23]. As a peculiar characteristic of con-nective tissues, the crural fascia also shows a time-depend-ent behavior [26].

It is evident that the particular multilayered structural conformation allows the crural fascia to adapt and to main-tain structural compatibility during the traction of muscles [3, 21]. Alterations of the mechanical properties of fascia can be related to a number of painful syndromes, such as the acute and chronic exertional compartment syndrome related to an increase in pressure within a specific com-partment, more frequently the anterior. This pathology is

🖄 Springer

observed in athletes practicing sports disciplines characterized by repetitive loadings. It can be interpreted as a reduction in the capability of fascial tissue to adapt to variations in the shape of muscles. The hypothesis of the involvement of the crural fascia in this pathology is, however, still controversial [6, 12] and needs further investigation to be confirmed.

The literature on the characterization of crural fascia mechanics is far from being complete [6, 12, 26]. In order to increase the knowledge in this field, the present work aims to investigate, in particular, the elastic behavior by adopting a hyperelastic constitutive model reinforced by two families of collagen fibers. The experimental data here reported are obtained from mechanical tests from a previous study [17, 26]. The model fitting is performed through an optimization procedure implemented in a user-defined routine.

The constitutive model is implemented in a general-purpose finite element software (Abaqus, Dassault Systémes) via specific user subroutines. A transversal section of the lower limb is modeled with particular attention to the conformation of the internal regions. Different numerical analyses are developed to pinpoint the mechanical response with particular regard to the relationship between an increase in volume and the resulting rise in internal pressure in the muscle compartments, considering both the physiological and pathological levels of pressure.

2 Materials and methods

2.1 Crural fascia constitutive model

The mechanical conditions of the crural fascia considered in this work are characterized by a physiological range of strains. In addition, the internal pressure of the different compartments acts as a steady-state condition. Therefore, the mechanical response of the crural fascia can be described by means of a hyperelastic constitutive model. Because of the presence of specifically oriented collagen fibers, a fiber-reinforced constitutive model is assumed that considers an isotropic ground matrix reinforced by two groups of collagen fibers. According to histological analyses, these are considered to be mechanically equivalent. Locally, the two groups of collagen fibers show a symmetrical disposition relative to the proximal–distal (P–D) and the medial–lateral (M–L) direction, with an average angle of about 40° (Fig. 1) relative to the P–D direction [26]. Because of the weak interaction between the two groups of fibers disposed on adjacent layers, it is assumed that the strain energy function can be dependent on a limited
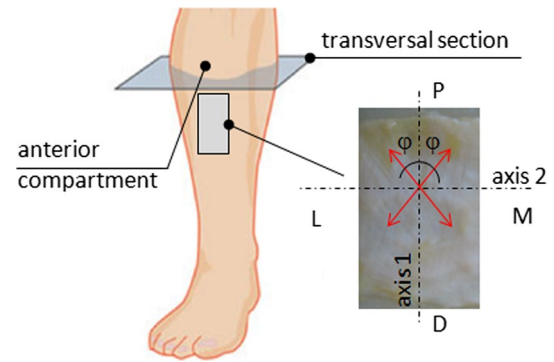

Fig. 1 Lower limb region with a representation of a sample of crural fascia from the anterior compartment. The collagen fiber disposition relative to the proximal distal (P–D) and medial lateral (M–L) directions is indicated

number of invariants [11] in relation to the general formulation [20]:

$$W = W(I_1, I_3, I_4, I_6) \tag{1}$$

where the invariants are defined as:

$$I_1 = \text{tr}(\mathbf{C}), \quad I_3 = J^2 = \det(\mathbf{C}),$$
$$I_4 = \mathbf{C} : (\mathbf{m}_0 \otimes \mathbf{m}_0), \quad I_6 = \mathbf{C} : (\mathbf{n}_0 \otimes \mathbf{n}_0) \tag{2}$$

being $\mathbf{C}$ the Cauchy–Green strain tensor $\mathbf{C} = \mathbf{F}^T\mathbf{F}$ and $\mathbf{F}$ the deformation gradient. The scalars I_1 and I_3 are principal invariants of the right Cauchy–Green tensor, J is the deformation gradient, and I_4 and I_6 are structural invariants dependent on the initial collagen fiber disposition, defined by the unit vectors $\mathbf{m}_0$ and $\mathbf{n}_0$, respectively. An additive contribution to the strain energy function of ground matrix W_m and collagen fibers W_f is considered here:

$$W = W_\text{m}(I_1, I_3) + W_\text{f}(I_4, I_6) \tag{3}$$

Because of the large water content, it is assumed that the tissue behaves like an almost-incompressible material. Therefore, the following form for the strain energy function is proposed:

$$W = U_\text{m}(J) + \tilde{W}_\text{m}\left(\tilde{I}_1\right) + \tilde{W}_\text{f}\left(\tilde{I}_4, \tilde{I}_6\right) \tag{4}$$

splitting the material contribution in volumetric and iso-volumetric parts. The modified invariants indicated in (4) are obtained by substituting the right Cauchy–Green strain tensor with its iso-volumetric part, defined as $\tilde{\mathbf{C}} = J^{-2/3}\mathbf{C}$. The hydrostatic term is used as a penalty term to ensure an almost incompressibility of the tissue. A specific form of the strain energy function is defined as:

$$W = \frac{k_v}{2}\left(J^2 - 2\ln J\right) + \frac{\mu}{2}\left(\tilde{I}_1 - 3\right) + \frac{k_m}{2\alpha_m}\left\{\exp\left[\alpha_m\left(\tilde{I}_1 - 3\right)\right]\right.$$
$$\left. - \alpha_m\left(\tilde{I}_1 - 3\right) - 1\right\} + + \frac{k}{2\alpha_f}\left\{\exp\left[\alpha_f\left(\tilde{I}_4 - 1\right)\right]\right.$$
$$\left. - \alpha_f\left(\tilde{I}_4 - 1\right) - 1\right\} + + \frac{k_f}{2\alpha_f}\left\{\exp\left[\alpha_f\left(\tilde{I}_6 - 1\right)\right]\right.$$
$$\left. - \alpha_f\left(\tilde{I}_6 - 1\right) - 1\right\} \tag{5}$$

being k_v the bulk modulus, μ, c and α_m terms related to the mechanical response of the ground matrix and k_f and α_f terms related to the mechanical response of specifically oriented collagen fibers. The terms μ, k_v, k_m and k_f are stress-like parameters, while α_m and α_f are dimensionless. The latter parameters account for the nonlinear response of ground matrix and oriented collagen fibers. The exponential terms of Eq. (5) are considered only in the case of a tensile strain to account for the null contribution of the crimped collagen fibers in compression. The stress is obtained in terms of the second Piola–Kirchhoff stress tensor through the derivative of the strain energy function (5) relative to the right Cauchy–Green strain tensor $\mathbf{C}$:

$$\mathbf{S} = 2\frac{\partial W}{\partial \mathbf{C}} = Jp\mathbf{C}^{-1} + \tilde{\mathbf{S}}_m + \tilde{\mathbf{S}}_f \tag{6}$$

where the hydrostatic pressure p and the two tensors of the right-hand side are given by:

$$p = k_v\left(J - \frac{1}{J}\right)$$
$$\tilde{\mathbf{S}}_m = \left\{\mu + k_m\exp\left[\alpha_m\left(\tilde{I}_1 - 3\right) - 1\right]\right\}\left[\mathbf{I} - \frac{I_1}{3}\mathbf{C}^{-1}\right]$$
$$\tilde{\mathbf{S}}_f = k_f\left\{\exp\left[\alpha_f\left(\tilde{I}_4 - 1\right)\right] - 1\right\}J^{-2/3}\left[\mathbf{n}_0 \otimes \mathbf{n}_0 - \frac{I_4}{3}\mathbf{C}^{-1}\right]$$
$$+ k_f\left\{\exp\left[\alpha_f\left(\tilde{I}_6 - 1\right)\right] - 1\right\}J^{-2/3}\left[\mathbf{m}_0 \otimes \mathbf{m}_0 - \frac{I_6}{3}\mathbf{C}^{-1}\right] \tag{7}$$

2.2 Constitutive model fitting

The constitutive model is fitted to the mechanical response of the tissue making reference to uniaxial independent tensile tests along the P–D and the M–L directions that are recognized as the symmetrical axes with respect to the initial disposition of the fibers. Because of the aspect ratio of the specimens adopted in the tests [17, 26], a uniaxial stress condition is considered to be an acceptable approximation of the mechanical state. The kinematics constraint of incompressibility is considered to obtain non-null stress components as a function of the stretches in the plane of membrane. The stress component of the second Piola–Kirchhoff stress along the loading direction is deduced from the nominal stress P as $S = P/\lambda$, where λ is the stretch along the direction of elongation. The collagen fiber

orientation in the initial configuration is defined by the unit vectors $(\cos\varphi, \sin\varphi, 0)$ and $(\cos\varphi, -\sin\varphi, 0)$, being φ the fiber angle of 40° relative to the P–D direction (Fig. 1). The strain energy function depends on a set of five constitutive parameters $\boldsymbol{\eta} = (\mu, k_m, \alpha_m, k_f, \alpha_f)$. The optimum set $\boldsymbol{\eta}_{opt}$ is obtained by the minimization of a scalar function that estimates the error between the numerical results and experimental data:

$$\Phi(\boldsymbol{\eta}) = \left\{\left[\Phi_{P-D}(\boldsymbol{\eta})\right]^2 + \left[\Phi_{M-L}(\boldsymbol{\eta})\right]^2\right\}^{1/2} \tag{8}$$

where the two terms are given, respectively, by:

$$\Phi_{P-D}(\boldsymbol{\eta}) = \frac{1}{N_{P-D}}\sum_{i=1}^{N_{P-D}}\left[1 - S_{l,i}^{exp}\left(\lambda_{l,i}^{exp}\right)\Big/S_1\left(\boldsymbol{\eta}, \lambda_{l,i}^{exp}, \lambda_{2,i}\right)\right]^2 \tag{9}$$

$$\Phi_{M-L}(\boldsymbol{\eta}) = \frac{1}{N_{M-L}}\sum_{i=1}^{N_{M-L}}\left[1 - S_{2,i}^{exp}\left(\lambda_{2,i}^{exp}\right)\Big/S_2\left(\boldsymbol{\eta}, \lambda_{l,i}, \lambda_{2,i}^{exp}\right)\right]^2 \tag{10}$$

being N_{P-D} and N_{M-L} the number of experimental values $(S_{j,i}^{exp}, \lambda_{j,i}^{exp})$ for the two independent tensile tests in the P–D and M–L direction, respectively. For each couple of experimental values, the membrane stretch perpendicular to the loading direction is obtained by imposing a null value of the corresponding stress component. The minimization procedure of the error function Φ is implemented with a user-defined routine [5, 16] in the software Scilab (Consortium Scilab, INRIA–ENPC).

2.3 Finite element analysis of limb behavior

2.3.1 Finite element model of lower limb section

A transversal segment of the lower limb at the medial third is modeled on the basis of anatomical data, as represented in Fig. 2. This section is characterized by a relatively simple connection of the crural fascia with surrounding structures, in particular with enwrapped muscles. The two-dimensional finite element model is created with Abaqus/CAE (Dassault Systémes). The model uses two-dimensional plane strain elements, with a hybrid formulation for tissues showing an almost-incompressible behavior. Frictionless contact conditions are considered in order to describe the possible sliding of the deep fascia with surrounding tissues, namely muscles and fat tissues.

2.3.2 Constitutive models for lower limb tissues

For the crural fascia, the hyperelastic and fiber-reinforced constitutive model presented in the previous section is considered, while the other tissues are defined according to
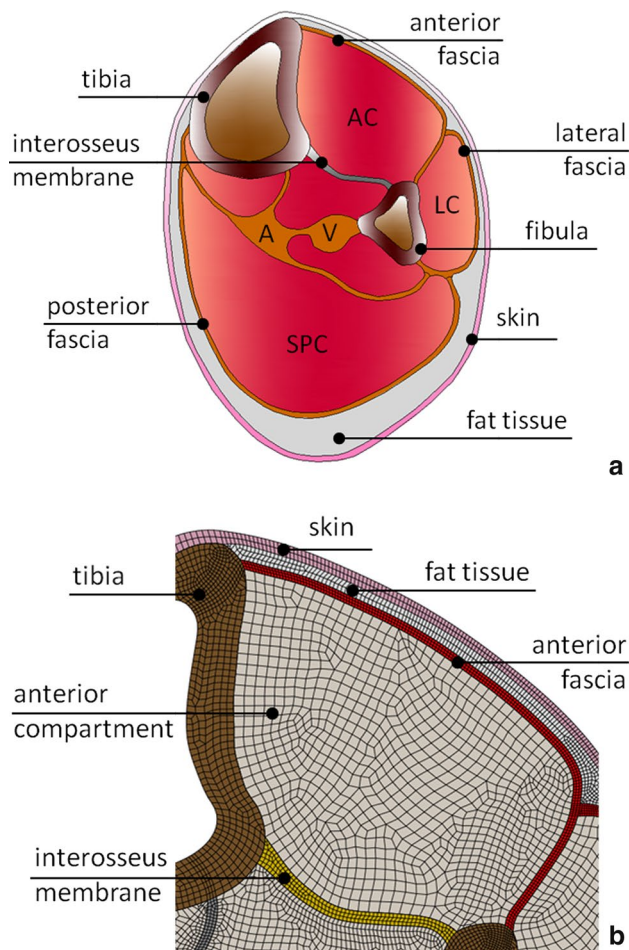
Fig. 2 Representation of the transversal section (**a**) of the lower limb, as indicated in Fig. 1 (*AC*, anterior compartment; *LC*, lateral compartment; *SPC*, superficial posterior compartment; *V*, vein; *A*, artery) and details of the corresponding two-dimensional finite element model of the anterior region (**b**)

data taken from the literature. The tibia and fibula cortical bone is assumed to be orthotropic and linear elastic [15]. The interosseus membrane is considered as linear elastic with Young's modulus of 600 MPa and Poisson's ratio of 0.3 [18]. Skin [1] and fat tissues [8] are considered as incompressible and linear elastic with Young's modulus of 0.72 and 0.00321 MPa, respectively. The properties of blood vessels and their surrounding soft envelopment are homogenized, as a reasonable simplification, assuming fat elastic properties. Muscles are described as poro-elastic material with shear modulus of 0.0083 MPa [13], permeability of 100 mm² kPa⁻¹ s⁻¹ and porosity corresponding to a blood volume fraction of about 8 % [27]. Particular attention is paid to the constitutive modeling of the crural fascia because it is considered as the most involved structure in determining the enwrapping effect of the muscle compartments and the possible increase in intra-compartmental pressure.

2.3.3 Boundary and loading conditions

The internal surfaces of the tibia and fibula are considered to be fixed. The internal pressure induced in the lower limb is simulated with a nonlinear analysis by imposing an incremental pore pressure in the muscles and determining a consequent volumetric expansion, with impervious contact surfaces between muscles and adjacent regions. In order to mimic the physiological basal condition, in the muscle a pore pressure corresponding to a physiological compartment pressure of 14 mmHg is applied [7]. The analysis of the effects of a compartment internal overpressure is then performed by considering three loading conditions. In the first loading condition, an internal pressure of 100 mmHg is applied in the anterior compartment, while maintaining an internal pressure of 14 mmHg in the other compartments. In the second loading condition, an internal pressure of 100 mmHg is applied in the posterior compartment, with internal pressure of 14 mmHg in the other compartments. Finally, in the third loading condition an internal pressure of 100 mmHg is applied in the anterior compartment with an internal pressure of 14 mmHg in the posterior compartment and 25 mmHg in the lateral compartment, the aim being to understand the possible effects of an overpressure in the lateral region. The internal pressure of 100 mmHg represents the highest pathological pressure value according to the literature [7].

3 Results

Figure 3 reports the comparison of numerical results with experimental data. These data refer to uniaxial tensile tests, for both the anterior (Fig. 3a, b) and the posterior compartments (Fig. 3c, d). The constitutive parameters obtained by the fitting procedure indicated in the previous section are reported in Table 1.

Figure 4 shows the magnitude of displacement contours on the deformed configurations of the lower limb section obtained at an intermediate step of the three loading conditions analyzed. Figure 4a refers to an internal pressure of 50 mmHg acting in the anterior compartment, while Fig. 4b refers to an internal pressure of 50 mmHg in the posterior. Finally, Fig. 4c refers to internal pressures of 50 and 25 mmHg acting simultaneously in the anterior and lateral compartments, respectively. The magnitude displacement fields at the same level of internal pressure are shown in Fig. 5 by means of vectors plotted on the deformed configuration. For a better visualization, only crural fascia, tibia, fibula and the interosseus membrane are shown.

The graph of Fig. 6 shows the internal pressure in the anterior and posterior muscle compartments versus the change in a normalized equivalent radius for the three
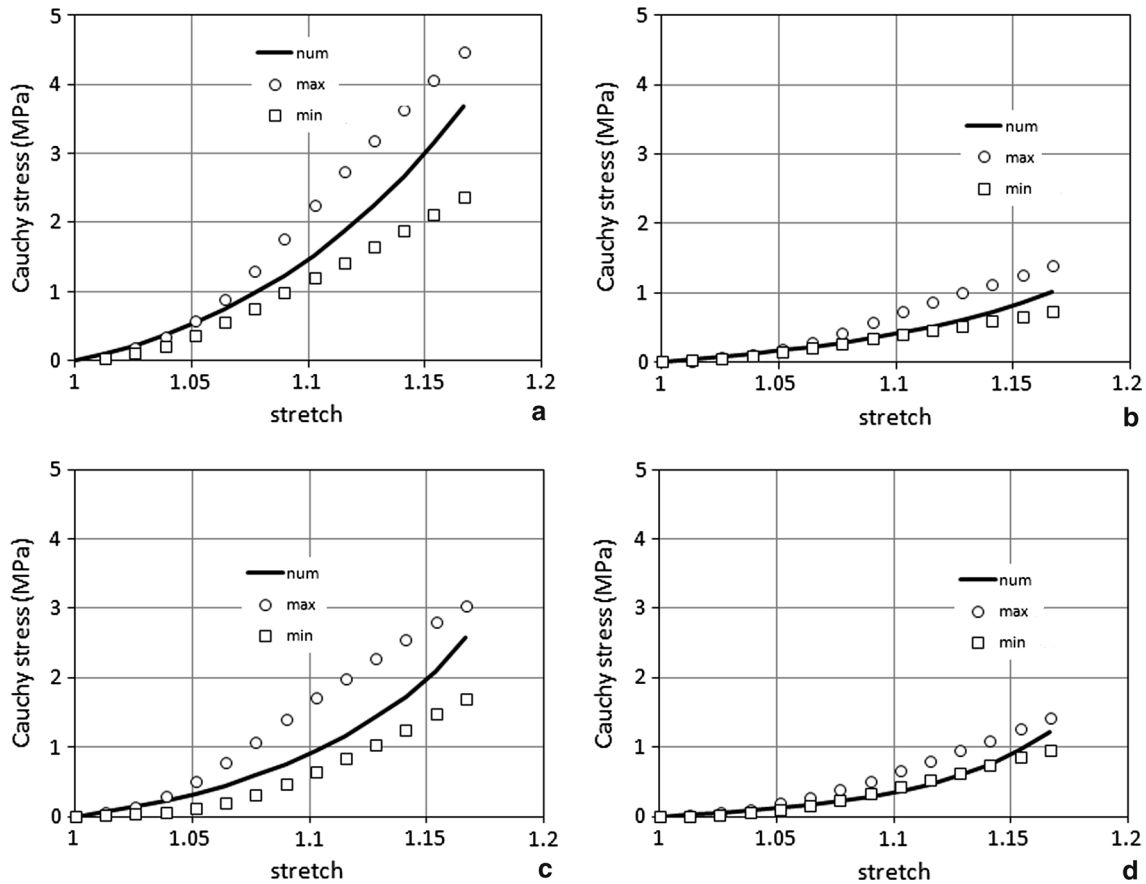
Fig. 3 Stress–strain behavior for the crural fascia in terms of Cauchy stress versus stretch. The *curves* related to the numerical model are reported as *solid lines*, while *open circles* and *squares* represent experimental data for the highest and lowest stiffness of the sam-ples, respectively. Data are reported for the anterior compartment in the proximal–distal (**a**) and medial–lateral direction (**b**) and for the posterior compartment in the proximal–distal (**c**) and medial–lateral direction (**d**)

Table 1 Constitutive parameters for crural fascia of anterior and posterior compartments obtained by the best fit of the experimental tensile tests along proximal–distal and medial–lateral directions

	k_m (MPa)	α_m	k_f (MPa)	α_f
Anterior	1.094	6.357	10.070	1.470
Posterior	0.728	14.933	6.319	1.251

loading conditions analyzed. The equivalent radius is defined by taking the square root of a muscle compartment transversal area; therefore, this measure is related to the compartment volume enwrapped by crural fascia and adjacent structures. The relationship between internal pressure and change in normalized equivalent radius provides a representation of the fascia stiffness. The equivalent radius is normalized to its value in physiological conditions, conventionally set at 14 mmHg. The gray region represents the range of internal pressure in which the compartment syndrome can arise.

4 Discussion

The constitutive model adopted provides a suitable description of the mechanical response of the crural fascia, as shown in Fig. 3. Along P–D direction, the tissue shows greater membrane stiffness in the anterior compartment than in the posterior. In general, the same difference can be found for the mechanical response in M–L direction, but in a limited range of strain, the samples harvested from the anterior and posterior compartments have similar response in M–L direction [2, 26].

In spite of the fact that the crural fascia of the anterior and posterior compartments shows similar values of membrane stiffness in M–L direction within a limited range of strains, the posterior compartment is more deformable because it is characterized by a larger diameter than the anterior compartment. At present, there are no histological analyses available for the comparison of the anterior and posterior compartment tissues to help in the clarification of the strong difference in the mechanical response. However,
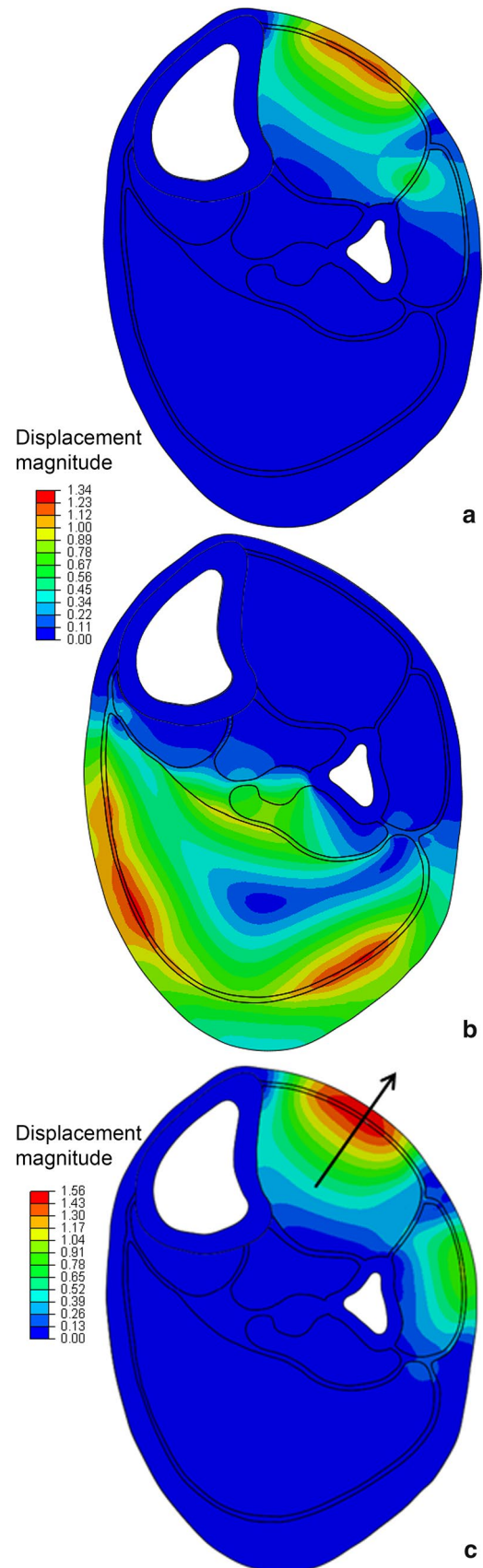
Fig. 4 Magnitude displacements (mm) reported on the deformed ▶ configuration of the lower limb. **a** 50 mmHg internal pressure applied in the anterior compartment. **b** An internal pressure of 50 mmHg applied in the posterior compartment. **c** Internal pressure of 50 mmHg applied in the anterior compartment and 25 mmHg internal pressure in the lateral compartment. The *arrow* represents the direction for the experimental measurement of the volume variation, according to [9]

during the dissection it was observed that tissues from the anterior compartment show a greater and denser number of collagen fiber fascicles suggesting a stiffer response. This is confirmed also by the numerical analyses, showing how posterior compartment undergoes greater displacements than the anterior at the same level of internal pressure (Figs. 4a, b, 5a, b). The numerical model shows also that the anterior compartment finds a lateral confinement due to the presence of high stiffness regions, as tibia, interosseus membrane and fibula. On the contrary, the posterior compartment can find major adaptability inducing a deformation of the internal compartments, as shown by the magnitude displacement fields.

The graph of Fig. 6 is in agreement with describing the greater compliance of the posterior compartment. In fact, at the same level of normalized equivalent radius the internal pressure of the anterior compartment is greater than in the posterior. This characteristic is evident also in clinical findings that highlight a higher occurrence of the compartment syndrome in the anterior region of the leg.

The internal pressure imposed in the numerical analyses is in the range of experimental values reported in the literature [10, 14, 28]. Because of the high intersubject variability, it is difficult to establish a precise threshold of intra-compartment pressure inducing a compartment syndrome. According to some authors, a pathologic condition can be identified at a pressure of about 30 mmHg [10, 14], while other authors adopt higher limits considering as pathological values in excess of 40 mmHg [28]. French and Price [7] reported in their study that normal values at rest for anterior intra-compartment pressure ranged from 2.2 up to 25.7 mmHg, with a raise up between 6.6 and 49.3 mmHg after exercise. In the following rest, they observed that pressure decreased rapidly to the initial values in a few minutes. On the contrary, pathological cases showed an intra-compartment pressure after exercise ranging from 58.1 up to 100 mmHg. In the light of these data, the interval assumed for the intra-compartment pressure ranges from 14 mmHg, regarded as average value for the physiological condition, up to 100 mmHg that represents the highest peak found in pathological cases.

The deformation of the anterior compartment has been experimentally measured [9] by evaluating the variation in the equivalent radius along the direction indicated in Fig. 4c, for a change in intra-compartment pressure from
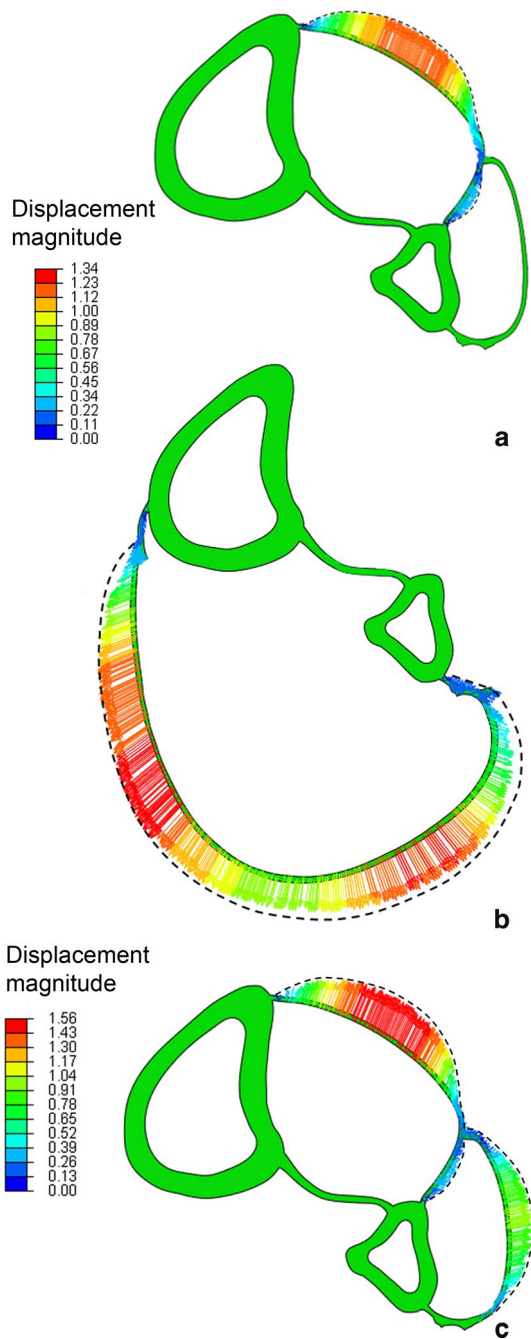
Fig. 5 Magnitude displacements (mm) represented by vectors plotted on the deformed configuration. **a** 50 mmHg internal pressure applied in the anterior compartment. **b** Internal pressure of 50 mmHg applied in the posterior compartment. **c** Internal pressure of 50 mmHg applied in the anterior compartment and 25 mmHg internal pressure in the lateral compartment

Fig. 6 Internal pressure in the anterior and posterior compartments versus a change in normalized equivalent radius. The pressure of the anterior compartment is calculated assuming a physiological pressure (*dark gray*) and pressure of 25 mmHg (*light gray*) in the lateral compartment (LC). The *gray area* identifies the pressure range in which the compartmental syndrome can arise

physiological to pathological values. Measurements on different subjects by means of ultrasound tests have shown a percentage variation in the anterior compartment diameter in the range 5.8–9 % with respect to the basal condition. The numerical a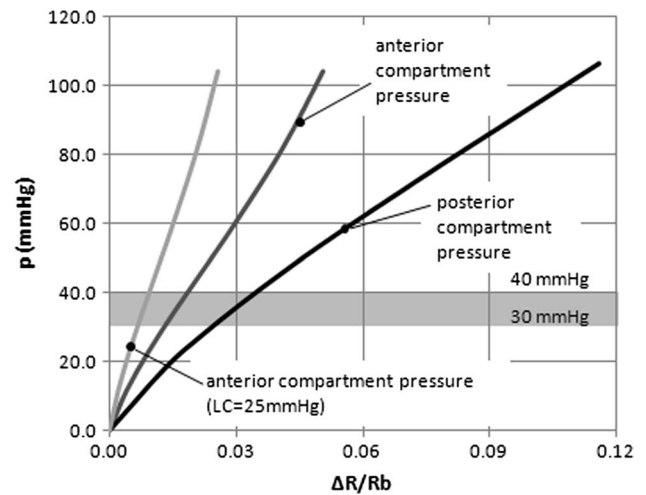nalyses conducted applying internal pressure similar to that of experimental conditions in the anterior compartment (50–60 mmHg) show a percentage increase in the compartment diameter ranging from 5.6 to 7.6 %, compared with the basal condition. This range is in agreement with the literature [9], confirming the reliability of the numerical model developed.

It is assumed that the stiffness of the crural fascia is not related with compartment syndrome [6] because sometimes measurements indicate that the fascia has greater stiffness in some healthy subjects than in others affected by compartment syndrome. In reality, the problem requires a more in-depth investigation for a number of reasons. In fact, while the experimental data reported [6] refer to longitudinal stiffness, the numerical analyses show that it is the circumferential stiffness that plays an important role in the adaptation of enwrapped muscles. Therefore, the investigation should be addressed further to the behavior of the crural fascia along the medial–lateral direction. Moreover, the large variation in internal pressure among different subjects suggests that the physiological range of internal pressure and, consequently, a possible compartment syndrome is patient specific. For this purpose, the possibility of investigating the interaction phenomena through parametric analyses on the basis of the numerical model developed seems appealing.

The investigation into the interaction of crural fascia with enwrapped muscles was in the past considered using simplified numerical models which could only approximate mechanical conditions under the simple hypothesis of the spherical shape of the compartments [12]. While

this could be acceptable for the posterior compartment, it is more appropriate to assume single curvature geometry for the anterior compartment, as proposed in the present work. The same hypothesis is probably more acceptable for the lateral compartment, too. In addition, previous numerical approaches considered the crural fascia as linear and isotropic material, while in the present approach a constitutive model has been adopted that is more consistent with the nonlinear and anisotropic behavior of this tissue.

Clinical data show that the increase in volume in the compartment is the cause of the pressure rise and, therefore, of compartment syndrome. On the other hand, in the numerical analyses the increase in pressure is considered to be the cause of volume change. However, since the two terms are related to one other, the numerical model offers a suitable representation of the mechanical conditions that could favor the rise in pathological conditions, for example an alteration in crural fascia stiffness. It is likely that the use of a numerical approach could also help in evaluating the effects of different prestress conditions along the P–D direction on the M–L membrane stiffness. This is a further unknown issue because of the difficulty in determining the stretch condition of the fascia in the P–D direction by means of experimental investigation.

Assuming a hyperelastic constitutive model, viscous phenomena and the dependency of the mechanical response of the crural fascia on the loading rate are not considered in this work. However, it must be pointed out that the present analyses refer to a steady-state condition in which the time-dependent phenomena can be regarded as completely developed. Consequently, the numerical model proposed allows for obtaining a feasible representation of the mechanical behavior of the crural fascia. Nonetheless, the model represents the starting point for future advances, to evaluate a time-dependent response associated with physiological behavior under muscular contraction. This also implies the development of a more accurate three-dimensional model.

References

1. Annaidh AN, Bruyère K, Destrade M, Gilchrist MD, Otténio M (2013) Characterising the anisotropic mechanical properties of excised human skin. J Mech Behav Biomed Mater 5(1):139–148
2. Azizi E, Halenda GM, Roberts TJ (2009) Mechanical properties of the gastrocnemius aponeurosis in wild turkeys. Integr Comp Biol 49(1):51–58
3. Benettazzo L, Bizzego A, De Caro R, Frigo G, Guidolin D, Stecco C (2010) 3D reconstruction of the crural and thoracolumbar fasciae. Surg Radiol Anat 33:855–862
4. Benjamin M (2009) The fascia of the limbs and back: a review. J Anat 214:1–18
5. Corana A, Marchesi M, Martini C, Ridella S (1987) Minimizing multimodal functions of continuous variables with the simulated annealing algorithm. ACM Trans Math Softw 13(3):262–280
6. Dahl M, Hansen P, Stål P, Edmundsson D, Magnusson SP (2011) Stiffness and thickness of fascia do not explain chronic exertional compartment syndrome. Clin Orthop Relat Res 469:3495–3500
7. French EZ, Price WH (1962) Anterior tibial pain. Br Med J 2:1290
8. Geerligs M, Peters WMG, Ackermans PAJ, Oomens CWJ, Baaijens FTP (2008) Linear viscoelastic behavior of subcutaneous adipose tissue. Biorheology 45:677–688
9. Gershuni DH, Gosink BB, Hargens AR, Gould RN, Forsythe JR, Mubarak SJ, Akeson WH (2011) Ultrasound evaluation of the anterior musculofascial compartment of the leg following exercise. Clin Orthop Relat Res 10:59–65
10. Hargens AR, Schmidt DA, Evans KL, Gonsalves MR, Cologne JB, Garfin SR, Mubarak SJ (1981) Quantitation of skeletal-muscle necrosis in a model compartment syndrome. J Bon Joint Surg Am 63(4):631–636
11. Holzapfel GA, Gasser TC, Ogden RW (2000) A new constitutive framework for arterial wall mechanics and a comparative study of material models. J Elast 61:1–48
12. Hurschler C, Vanderby R, Martinez DA, Vailas AC, Turnipseed WD (1994) Mechanical and biomechanical analyses of tibial compartment fascia in chronic compartment syndrome. Ann Biomed Eng 22:272–279
13. Mattei CP, Beca S, Zahouani H (2008) In vivo measurements of the elastic mechanical properties of human skin by indentation tests. Med Eng Phys 30:599–606
14. Mubarak SJ, Owen CA, Hargens AR, Garetto LP, Akeson WH (1978) Acute compartment syndromes: diagnosis and treatment with the aid of the wick catheter. J Bon Joint Surg Am 60(8):1901–1905
15. Natali AN, Carniel EL, Pavan PG (2008) Constitutive modelling of inelastic behaviour of cortical bone. Med Eng Phys 30(7):905–912
16. Natali AN, Pavan PG, Stecco C (2010) A constitutive model for the mechanical characterization of the plantar fascia. Connect Tissue Res 51(5):337–346
17. Pavan P, Stecco C, Pachera P, Natali AN (2012) Assessment of the mechanical properties of the human crural fascia. In: Cappozzo A, D'Alessio T, Guglielmelli E, Pennestrì E, Salinari S (eds) Congresso Nazionale di Bioingegneria. Patròn, Bologna, pp 191–192
18. Pfaeffle HJ, Toamino MM, Grewal R, Xu J, Boardman ND, Woo SL, Herndon JH (1996) Tensile properties of the interosseous membrane of the human forearm. J Orthop Res 14(5):842–845
19. Simmonds N, Miller P, Gemmel H (2010) A theoretical framework for the role of fascia in manual therapy. J Bodywork Mov Ther 16:83–93
20. Spencer AJM (1971) Theory of invariants. In: Eringen AC (ed) Continuum physics, vol 1. Academic Press, New York, pp 239–353
21. Stecco C, Porzionato A, Lancerotto L, Stecco A, Macchi V, Day JA, De Caro R (2008) Histological study of the deep fascia of the limbs. J Bodywork Mov Ther 12(3):225–230
22. Stecco A, Macchi V, Masiero S, Porzionato A, Tiengo C, Stecco C, Delmas V, De Caro R (2008) Pectoral and femoral fasciae: common aspects and regional specializations. Surg Radiol Anat 31(1):35–42
23. Stecco C, Pavan PG, Porzionato A, Macchi V, Lancerotto L, Carniel EL, Natali AN, De Caro R (2009) Mechanics of crural fascia: from anatomy to constitutive modelling. Surg Radiol Anat 31:523–529
24. Stecco S, Porzionato A, Lancerotto L, Stecco A, Macchi V, Day JA, De Caro R (2009) Anatomical study of myofascial continuity

in the anterior region of the upper limb. J Bodywork Mov Ther 13:53–62

25. Stecco C, Porzionato A, Lancerotto L, Stecco A, Masiero S, Day JA, De Caro R (2009) The pectoral fascia: anatomical and histological study. J Bodywork Mov Ther 13:255–261

26. Stecco C, Pavan PG, Pachera P, De Caro R, Natali AN (2013) Investigation of the mechanical properties of the human crural fascia and their possible clinical implications. Surg Radiol Anat pp 1–8, doi: 10.1007/s00276-013-1152-y (in press)

27. van Donkelaar CC, Huyghe JM, Vankan WJ, Drost MR (2001) Spatial interaction between tissue pressure and skeletal muscle perfusion during contraction. J Biomech 34:631–637

28. Warme WJ, Matesen FA (2013) Compartmental Syndromes. http://www.orthop.washington.edu/?q=patient-care/articles/shoulder/compartmental-syndromes.html. Accessed 26 Nov 2013